# Grain Refinement of AZ31 Magnesium Alloy by Titanium and Low-Frequency Electromagnetic Casting

YINGXIN WANG, XIAOQIN ZENG, WENJIANG DING, ALAN A. LUO, and ANIL K. SACHDEV

The grain-refinement effects of titanium (Ti) additions and a low-frequency electromagnetic casting (LFEC) process on the AZ31 magnesium alloy have been investigated. It is shown that Ti has no effect on the formation and distribution of secondary phases in the AZ31 alloy. The results suggests that the grain size decreases with an increasing cooling rate for the AZ31 alloy; it decreases first, however, then increases slightly for Ti-containing AZ31 alloys, indicating that the grain-refinement effect of Ti decreases with an increasing cooling rate. However, the grain size decreases first, and then increases with increasing Ti for a given cooling rate. The lowest grain size is obtained at the addition of about 0.01% Ti and the cooling rate of about 6 K/s. The grain refinement effect is explained in terms of the growth restriction factor (GRF) due to the constitutional undercooling generated by the Ti solute elements, which produces grain refinement up to a critical GRF value corresponding to about 0.01% Ti addition. The yield strength of a conventional-cast AZ31 alloy can be improved by grain refinement and expressed as $\sigma_y = 39.31 + 142.53\ d^{-1/2}$ according to the Hall–Petch relationship. The combination of the Ti grain refiner and the LFEC process during direct-chill (DC) casting of an AZ31 alloy can produce high-quality magnesium alloy billets with uniform and equiaxed grains of less than 40 $\mu$m across the billet section up to at least a 100-mm diameter, which further improves the yield strength of the alloy, resulting in $\sigma_y = 51.53 + 90.85\ d^{-1/2}$.

## I. INTRODUCTION

THE use of magnesium alloys for structural components in the automotive industry is attractive due to their excellent specific strength and low density. High-pressure die casting is currently the dominant process for magnesium automotive applications, but wrought magnesium alloys, *i.e.*, extrusions and sheet products, are receiving increasing attention from academia and industries due to their greater potential for vehicle mass reduction and performance improvement.[1,2] However, the cost of wrought magnesium products remains high due to the poor formability and low productivity associated with current magnesium extrusions and sheet products, and their formability and productivity are largely dependent on the quality of direct-chill (DC) casting billets.[3] Presently, there are several quality issues with magnesium alloy billets, such as macrosegregation, inclusions, porosity, coarse and asymmetric grains, and surface defects (liquation burl, stratification, and microcracks).

It is well known that a finer grain structure reduces the size of defects such as microporosity and secondary particles; therefore, grain refinement is an important technique for improving the quality of magnesium alloy billets. A variety of methods, such as superheating, agitation, and the addition of particles and solute elements, have been developed to refine the magnesium alloys.[4–6] The grain-refinement effects of the Al-4Ti-5B master alloy[4] and Sr as a solute element[6] in AZ31 alloy have been studied. It was found that it was very difficult to achieve dissolution of the Al-4Ti-5B master alloy, and the Sr additions to AZ31 led to the formation of acicular phase, which was detrimental to mechanical properties. Low-frequency electromagnetic casting (LFEC) processing is very effective in refining billet grain size, eliminating the macrosegregation, improving the temperature distribution during solidification, and enhancing the casting velocity. The LFEC process has been used to fabricate high-quality Al-Zn-Mg-Cu,[7] AZ80,[8] and ZK60[9] alloy billets. There are few publications that discuss the effect of Ti additions on grain refinement of magnesium alloys, although Ti is an effective grain refiner of aluminum alloys.[10] Xue *et al.*[11] reported the grain-refinement effect of $Al_3Ti$ on pure Mg and AZ31 alloy. It is well known that $Al_3Ti$ is unstable at a melt temperature above 700 °C;[10] Ti as a solute element has an important role in the grain refinement of pure Mg and the AZ31 alloy. The current study aims to investigate the effects of Ti and LFEC process on the grain refinement of AZ31 magnesium alloy.

YINGXIN WANG, Doctoral Student, XIAOQIN ZENG, Associate Professor, and WENJIANG DING, Director, are with the National Engineering Research Center of Light Alloys Net Forming, Shanghai Jiao Tong University, Shanghai 200030, People's Republic of China. Contact e-mail: wyx119@sjtu.edu.cn ALAN A. LUO, Staff Research Engineer, and ANIL K. SACHDEV, Group Manager, are with the General Motors Research and Development Center, Warren, MI 48090-9055, USA.
Manuscript submitted November 27, 2006.
Article published online June 26, 2007.

## II. EXPERIMENTAL PROCEDURE

AZ31-alloy ingots were melted in an electric furnace using a mild steel crucible under a protective cover gas mixture of 0.3 pct $SF_6$ and 99.7 pct $CO_2$, using pure Mg (99.95 pct) and Al (99.7 pct) ingots; Mn was also added in the form of an Al-Mn master alloy. Ti was added to the melt at 963 K in the form of the Al-10Ti master alloy, held for 30 minutes, and then stirred for 2 minutes at 1023 K. The melt was then poured at 993 K into a mild steel step-mold[6] preheated to 473 K. The chemical compositions of the investigated alloys are listed in Table I.

The melting of AZ31 alloy for DC casting was carried out in an electrical furnace using a mild steel crucible of 50 Kg under a protective gas. The melt was held at 1003 to 1013 K and cast at 943 to 948 K into billet with a diameter of 100 mm at a velocity of 180 to 200 mm/min, with a water-cooling flow of 0.025 $m^3$/min. The schematic diagram of the LFEC apparatus and the processing details were given by Dong *et al.*[7] The electromagnetic field was applied through the induction coil with an electrical current ranging from 50 to 150 A and frequency from 10 to 30 Hz.

Samples were sectioned from 15 mm near the edge of the step ingots, from 10 mm near the edge and in the center of the DC billet, for the as-cast microstructure observation. The samples for heat-treated microstructures were solutionized in a sulfur atmosphere at 723 K for 10 hours, followed by quenching in cold water. Characterization of the grain size and qualitative image analysis were conducted on selected specimens using an XJL-03 optical microscope (OM), Nanjing Jueyu Ltd; Shanghai Jiao Tong University and a JSM-5600LV scanning electron microscope (SEM), JEOL Ltd, Japan; Shanghai Jiao Tong University equipped with an Oxford energy-dispersive X-ray (EDX) detector, Oxford-Link ISIS; Shanghai Jiao Tong University.

The linear intercept method was used to measure the average grain size. Tensile specimens with a gage section of $4 \times 2 \times 15$ mm were cut from the step ingots, DC and LFEC billets, using electric-spark machining, and tensile testing was performed in a Zwick/Roell material test machine, Zwick Co. Ltd, Germany; Shanghai Jiao Tong University, using a constant cross-head speed of 1 mm/s at room temperature.

## III. RESULTS

### A. *Microstructures for Step Specimens*

Figure 1 shows the SEM images of AZ31 and AZ31-0.05Ti alloys at a cooling rate of 10 K/s. In both alloys, block-shaped secondary phases are present in the α(Mg) matrix with a size of 3 to 7 $\mu$m. The EDX analyses show that these particles contain Mg, Al, and Zn. The atomic percentage of Mg, Al, and Zn of these particles in the AZ31 alloy is 82.33, 16.20, and 1.47 (average of seven different areas), respectively. Similar results, 81.07 pct Mg, 17.79 pct Al, and 1.14 pct Zn, were found in the AZ31-0.05Ti alloy, indicating that these phases are the Zn-rich $Mg_{17}Al_{12}$ $\beta$ phases[4] in both cases. There are no obvious differences in the morphology and size of those particles in both alloys, *i.e.*, Ti has no significant effect on the formation and distribution of secondary phases in AZ31 alloy.

Figure 2 shows the as-cast microstructure of AZ31 and AZ31-0.05Ti alloys at cooling rates of 3 and 10 K/s. At the lower cooling rate, there are a few block-shaped Zn-rich $\beta$-phase particles of about 5 to 10 $\mu$m in both alloys (Figures 2(a) and (b)). The volume of Zn-rich $\beta$ particles increases, but with a reduced size, due to the higher cooling rate (Figures 2(c) and (d)).

Figure 3 shows the solutionized microstructure of the alloys solidified at a cooling rate of 6 K/s. It can be seen

**Table I. Chemical Compositions of Experimental Alloys (Mass Fraction Percent)**

| Nominal Alloy | Al | Zn | Mn | Ti | Cu | Ni | Fe | Mg |
|---|---|---|---|---|---|---|---|---|
| AZ31 | 2.94 | 0.91 | 0.20 | — | 0.002 | 0.002 | 0.006 | balance |
| AZ31-0.01Ti* | 3.11 | 0.93 | 0.19 | 0.002 | 0.001 | 0.002 | 0.006 | balance |
| AZ31-0.03Ti* | 3.29 | 0.92 | 0.19 | 0.003 | 0.002 | 0.002 | 0.005 | balance |
| AZ31-0.05Ti* | 3.52 | 0.92 | 0.21 | 0.007 | 0.002 | 0.002 | 0.003 | balance |

*The recovery rate of Ti was found to be very low, *i.e.*, 10 to 20 pct, with most of the Ti settled to the bottom of the crucible.
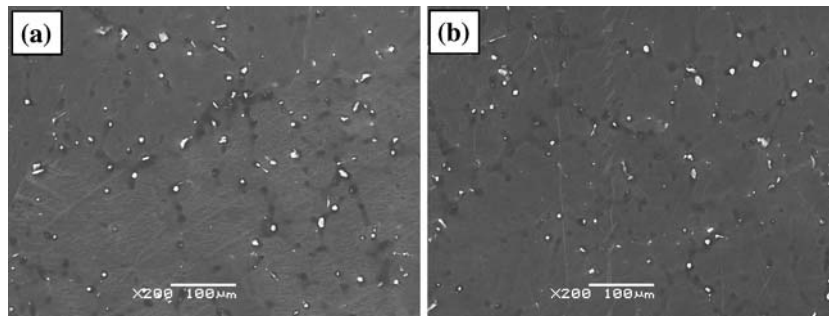


Fig. 1—SEM images of (*a*) AZ31 and (*b*) AZ31-0.05Ti alloys at a cooling rate of 10 K/s.
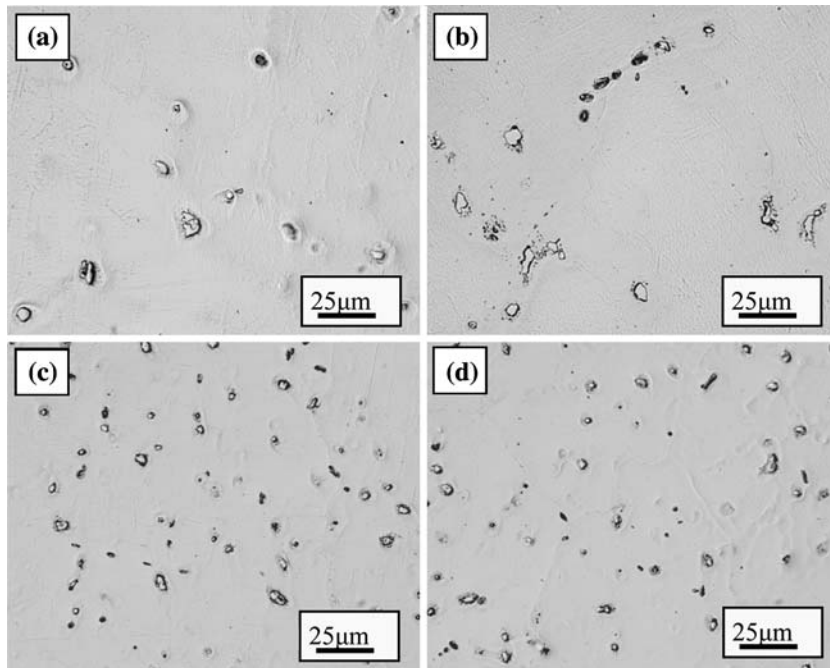
Fig. 2—Optical micrographs showing as-cast microstructure of (*a*) AZ31 and (*b*) AZ31-0.05Ti alloys at a cooling rate of 3 K/s; and (*c*) AZ31 and (*d*) AZ31-0.05Ti alloys at a cooling rate of 10 K/s.

that the grain size of AZ31 alloy decreases from the original 1100 ± 120 to 120 ± 10 $\mu$m for the AZ31-0.01Ti alloy, then to 150 ± 15 $\mu$m for the AZ31-0.03Ti alloy, and finally increases to 600 ± 55 $\mu$m for the AZ31-0.05Ti alloy. Figure 4 shows the relationship between grain size and cooling rate for the alloys. The grain size decreases with the increasing cooling rate up to 6 K/s, and then increases slightly at a higher cooling rate for the Ti-containing alloys, which indicates that the grain-refinement effect of Ti decreases with an increasing cooling rate. For all cooling rates in this study, the grain size is significantly reduced by a Ti addition of 0.01 pct (nominal composition), and then increases with increasing Ti (Figure 5).

## B. *Microstructures for DC and LFEC Specimens*

To investigate the combined effect of the Ti and the LFEC processing on the grain refinement of the AZ31 alloy, the optimal Ti addition (0.01 pct) and LFEC parameters (frequency and current)[12] were selected. The conventional DC cast billets showed a gradient microstructure with relatively coarse dendrites in the center of the billet and large Zn-rich $\beta$ particles in the interdendritic regions (Figure 6(a)). The edge of the DC cast billet showed a more equiaxed grain structure with refined Zn-rich $\beta$ particles due to the higher cooling rate near the billet surface (Figure 6(b)). It is also obvious that a higher volume fraction of Zn-rich $\beta$ particles are present in the billet center compared to the edge, indicating macrosegregation in the DC-cast billets. When LFEC (30 Hz and 80 A) is applied, all Zn-rich $\beta$ particles are greatly refined across the billet section (center to edge) with a size of 3 to 4 $\mu$m and a uniform distribution in the $\alpha$(Mg) matrix. The macrosegregation

seems to be reduced as well (Figures 6(c) and (d)). The combined effect of the LFEC and the grain refiner (0.01 pct Ti) on the as-cast microstructure is shown in Figures 6(e) and (f) no change is apparent with only LFEC processing.

Figure 7 shows the grain-size of the as-homogenized DC and LFEC billets. For the DC AZ31 billet, the grain size in the center is about 110 ± 18 $\mu$m, larger than that of (51 ± 10 $\mu$m) the edge, due to the lower cooling rate. Compared to the conventional-cast AZ31 alloy (Figure 3(a)), the grain size of the DC-cast AZ31 alloy decreases obviously for the higher cooling rate. The homogenized grain size is much finer (46 ± 8 $\mu$m) and more uniform across the cross-section in the LFEC billet processed at 30 Hz and 80 A. With the addition of 0.01 pct Ti to the AZ31 alloy and the combination of that and the LFEC processing, the grain size in the billet center decreases further (25 ± 6 $\mu$m); the grain size at the edge increases compared to the single LFEC billet, as can be seen from Figure 8. It can also be concluded that the grain size of the Ti-adding AZ31 alloy increases to a certain extent at a higher cooling rate.

## C. *Mechanical Properties*

Figure 9 shows the mechanical properties of the as-cast alloys solidified at a cooling rate of 6 K/s and the DC- and LFEC-cast AZ31 billets. The effects of the Ti additions on the yield strength and elongation of these alloys are evident (Figure 9(a)). All Ti-containing AZ31 alloys have a higher yield strength than does AZ31 for the conventional casting, with the AZ31-0.01Ti alloy exhibiting the highest strength and elongation. The elongation decreases with increasing Ti content corresponding to the changing trend of grain size (Figure 5).
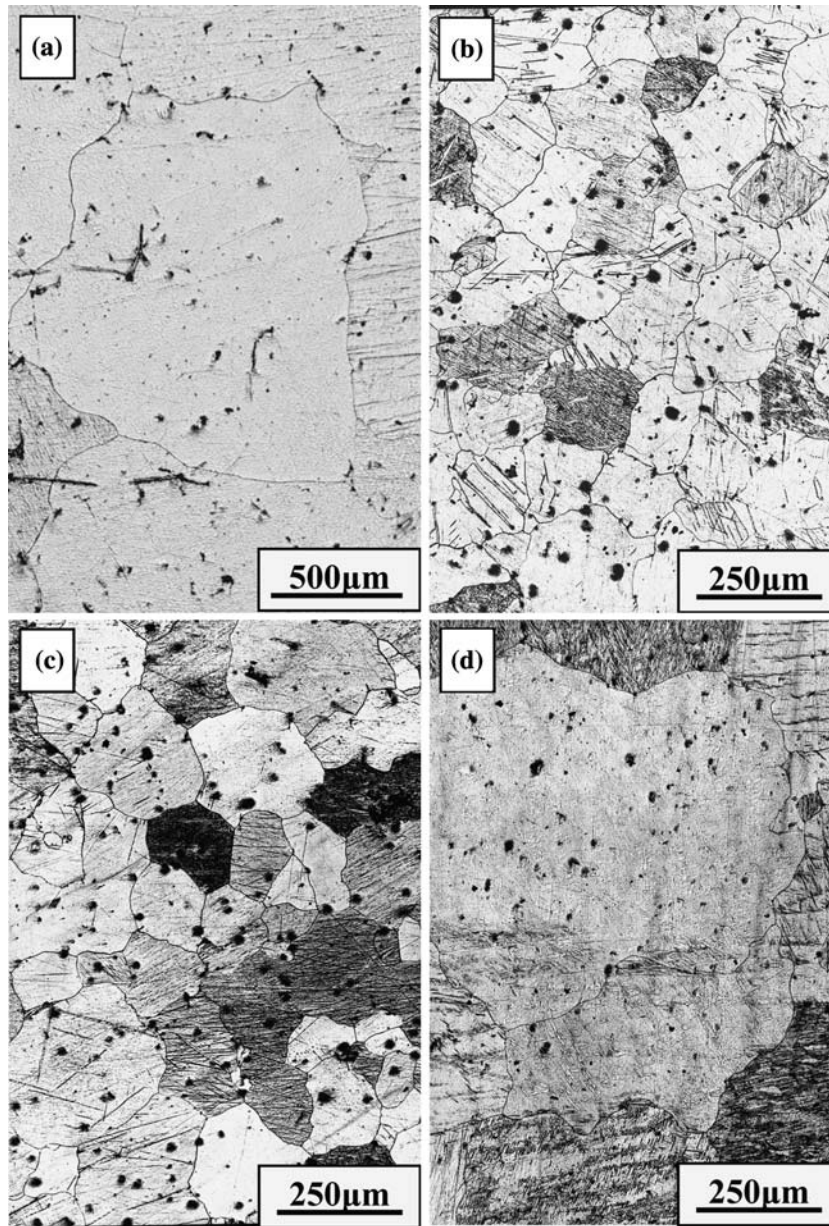
Fig. 3—Optical micrographs showing the solutionized microstructure of the alloys (*a*) AZ31, (*b*) AZ31-0.01Ti, (*c*) AZ31-0.03Ti, and (*d*) AZ31-0.05Ti solidified at a cooling rate of 6 K/s.[6]

Unlike the Sr-containing AZ31 alloys,[6] the finest grain size leads to the highest strength and elongation for the Ti-containing AZ31 alloys. After DC casting, the yield strength and elongation of the AZ31 alloy improve obviously (Figure 9(b)). The yield strength and elongation of the AZ31 alloy increase with an electromagnetic field applied at a frequency of 30 Hz and a current of 80 A, and that increases further with the combined 0.01 pct Ti addition and LFEC processing.

## IV. DISCUSSION

### A. *Microstructures for Step Specimens*

The effect of solute elements on grain refinement is in controlling the growth of the nucleated grains and the subsequent nucleation, which has been investigated in various aluminum alloy systems[13] and is explained in terms of the growth restriction factor (GRF) (GRF = $\sum_i m_i C_{0i}(k_i - 1)$, where $m_i$ is the slope of the liquidus line, $k_i$ is the distribution coefficient, and $C_{0i}$ is the initial concentration of element *i*). The constitutional undercooling generated by solute elements restricts grain growth by slowing the diffusion of the alloying elements in the solid/liquid interface. Some alloying elements, such as Al, Zr, Sr, Si, and Ca, have been reported to significantly refine pure magnesium, due to the relatively larger GRF value.[14] For different amounts of Al added to pure magnesium,[14] the larger GRF value leads to a finer grain size up to a critical GRF value; the relationship of the grain size and the GRF value is in accordance with a sigmoid, which can be denoted by
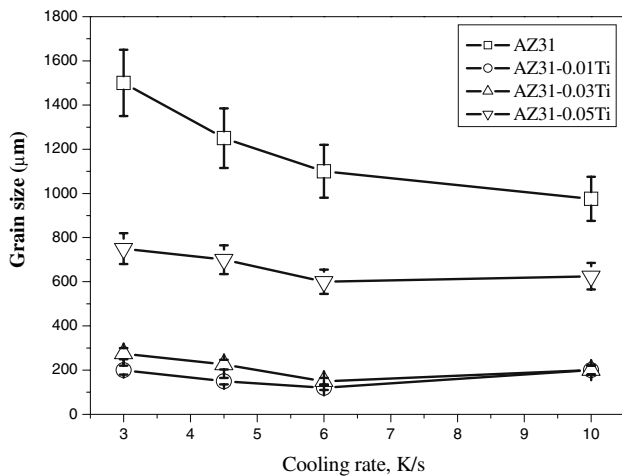
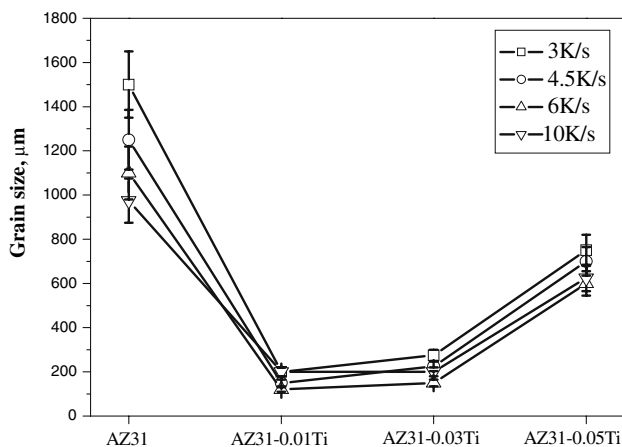Fig. 4—Grain size *vs* cooling rate for the experimental alloys.



Fig. 5—Grain size *vs* Ti content for the experimental alloys.

$Y_{grain\ size}$ = 587 + 887/(1 + exp (($x_{GRF}$ – 13)/3)), as can be seen from Figure 6 in Reference 4. The grain size is larger than that in Reference 14 because of the different cooling rate. Parameter $m(k – 1)$ of Al in magnesium is 4.32.[14] Therefore, the GRF value ($C_0 m(k – 1)$) of Al in the AZ31 alloy is 12.70 in this work. The AZ31-0.05Ti alloy has the maximum excess Al that is added by the master alloy, and the GRF value is 15.21. According to the relationship between the grain and the GRF value, the grain size of the AZ31 alloy with extra Al up to 0.58 is about 875 $\mu$m. Hence, the extra Al added by the master alloy is not likely to cause a significant change in grain size (Figures 3 through 5).

The Ti is the primary difference between the Ti-containing AZ31 alloys and the AZ31 alloy, which indicates that Ti can act as a high-efficient grain refiner for an AZ31 alloy. Figure 10 shows a binary-phase diagram of a Mg-Ti system.[15] In the corner of rich magnesium, there exists a peritectic reaction, Liquid + $\alpha$(Ti) $\leftrightarrow$ $\alpha$(Mg), at 651 °C. Since the grain refinement mechanism of Zr as a solute element is explained by the peritectic reaction,[14] this should also

hold true as the mechanism for grain refinement by Ti. The composition of the peritectic liquid is usually taken to be 0.002 wt pct Ti and that of the magnesium solute solution formed is 0.24 wt pct Ti. This gives an equilibrium distribution coefficient $k$ between the $\alpha$(Mg) and the liquid of ~120. Since the melting point of pure magnesium is 650 °C, the liquidus slope of the hypoperitectic region of the diagram, $m$, is ~500 K(wt pct)$^{-1}$. Therefore, the growth restriction parameter $m(k – 1)$ is around $5.95 \times 10^4$. The value of the growth-restriction parameter in the Mg-Ti system is four orders larger than that in Mg-Zr system,[14] which reveals that the prodigious constitutional undercooling ability of the Ti solute element leads to the high-efficient grain refinement of the AZ31 alloy.

During solidification of an alloy, the final grain size is determined by the balance of nucleation and growth that is controlled by the undercooling degree $\Delta T$, thereinto, $\Delta T = \Delta T_c + \Delta T_t + \Delta T_r$, where $\Delta T_c$ is the constitutional undercooling degree that is in direct proportion to the solute concentration, $\Delta T_t$, the thermal undercooling degree, is in direct proportion to the cooling rate, and $\Delta T_r$, the curvature undercooling degree, can be expressed as $\Delta T_r = 2\gamma T_m/L_v r$, where $\gamma$ is the interfacial free energy, $T_m$ is the local melting point, $L_v$ is the release of the latent heat per unit volume of the solidifying crystal, and $r$ is the dendritic tip radius.[16] In general, $T_m$ is affected by the solute concentration. However, for a peritectic system, the melting point increases with the increasing solute concentration (see the liquidus line). Hence, $\Delta T_r$ is also in direct proportion to the solute concentration. Figure 11 shows the relationship between the average dendritic growth rate (grain size) and the solute concentration.[17] In area I, with a thimbleful of solute, $\Delta T_t$ controls the grain size; in area II, with an increasing solute concentration, $\Delta T_c$ does, and in area III, with where the solute concentration is increased further, $\Delta T_r$ works. The $\Delta T_t$ plays an important role in the grain refinement for the AZ31 alloy without the Ti addition, which makes the grain size of the AZ31 alloy decrease with the increasing cooling rate (Figure 3). At a given cooling rate, *i.e.*, with an unchanged $\Delta T_t$, the addition of the 0.01 pct Ti solute, $\Delta T_c$ (GRF mechanism) plays an important role in the grain refinement, which leads to the finer grain size of the AZ31 alloy (Figure 4). While the dendritic-tip radius decreases as the Ti solute concentration increases further, due to a change in the growth mechanism of the dendrites, $\Delta T_r$ becomes the controlling parameter, which leads to the capillary phenomenon.[18] The capillary action improves the growth of the dendrites, resulting in the grain size increasing with the increasing Ti addition (Figure 4). In Figure 3, there exists a special condition, that is, the grain size of the AZ31-0.01Ti and AZ31-0.03Ti alloys increases again when the cooling rate exceeds 6 K/s. The increasing cooling rate will lead to a congregation of the Ti solute elements, which results in the increasing $\Delta T_r$ and, hence, the grain growth rate.

In general, the relationship between the grain size of the AZ31 alloy and the GRF value can be shown in Figure 12 that shows a critical GRF value after which the grain size
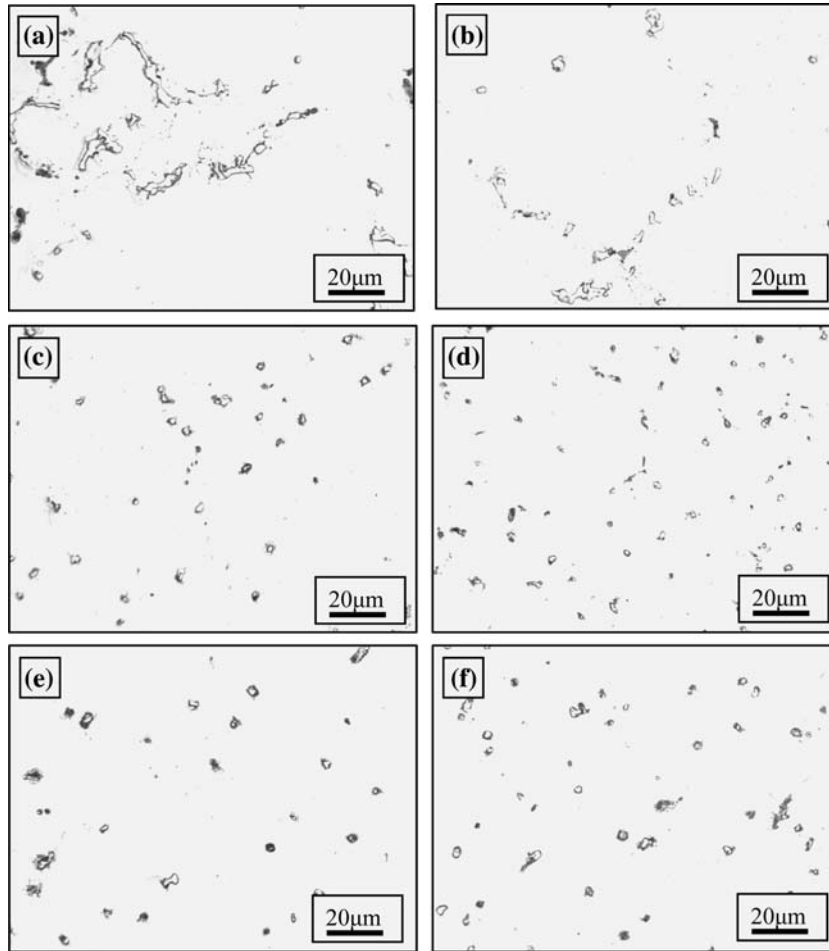
Fig. 6—Optical micrographs showing the as-cast microstructure in the center (*a*), (*c*), and (*e*) and at the edge (*b*), (*d*), and (*f*) of the DC and LFEC AZ31 alloys: (1) AZ31, DC (*a*) and (*b*); (2) AZ31, LFEC (30 Hz/80 A) (*c*) and (*d*); and (3) AZ31-0.01Ti, LFEC (30 Hz/80 A) (*e*) and (*f*).
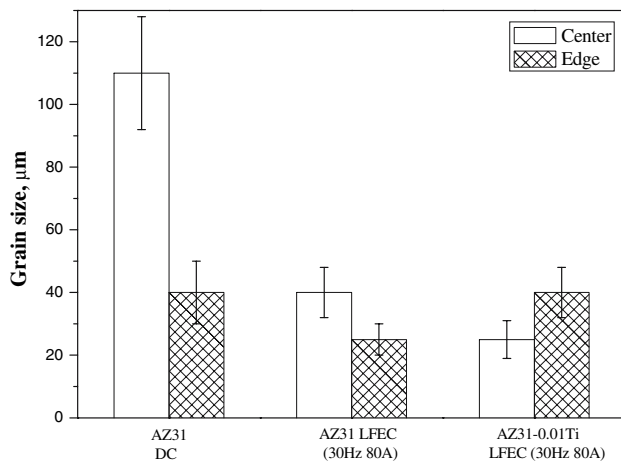


Fig. 7—Grain size measurements for AZ31 and AZ31-0.01Ti alloys prepared by DC and LFEC processing.

increases. Similar results were observed by Johnssons[17] in Ti grain refinement of pure Al despite a different critical GRF value reported for the aluminum system.

## B. *Microstructures for DC and LFEC Case Specimens*

In the conventional DC-cast AZ31 alloy, a deep liquid cave develops during the casting process, due to surface cooling and the gravity of the melt in the vertical casting machine, which results in a large temperature gradient across the billet cross section. At the billet edge, finer equiaxed grain and Zn-rich $Mg_{17}Al_{12}$ phases form (Figures 6(b) and 8(a)), due to the greater degree of undercooling caused by the huge cooling rate; in the billet center, the alloy melt retains the same liquid composition and existing no constitutional undercooling basically, which leads to the low nucleation probability of the $\alpha$(Mg) nucleus. After the nucleation of the $\alpha$(Mg) nucleus, dendritic growth takes place rapidly, forming coarse grain (Figure 8(b)). When the dendritic arms contact each other, the melt saturated with solutes congregates in the intergranular and in the end of the secondary dendritic arms, making it easy to form coarse $Mg_{17}Al_{12}$ phases and ($\alpha$-Mg + $Mg_{17}Al_{12}$) eutectics (Figure 6(a)). Due to the higher solute concentration in the center as compared to the edge, macrosegregation forms easily (Figures 6(a) and (b)).
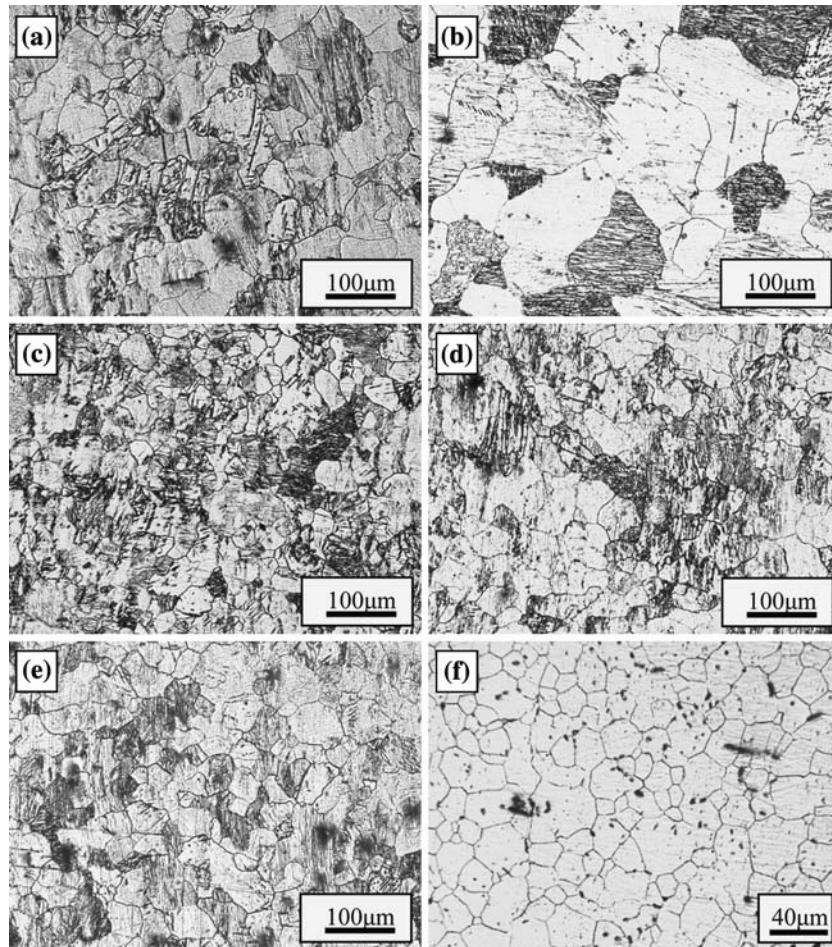
Fig. 8—Optical micrographs showing the as-solutionized microstructure at the edge (*a*), (*c*), and (*e*) and in the center (*b*), (*d*), and (*f*) of the AZ31alloy prepared by DC and LFEC processing: (1) AZ31, DC (*a*) and (*b*); (2) AZ31, LFEC (30 Hz/80 A) (*c*) and (*d*); and (3) AZ31-0.01Ti, LFEC (30 Hz/80 A) (*e*) and (*f*).

In the presence of an electromagnetic field, enhanced vertical convection reduces the temperature gradient obviously by bringing a lower temperature melt to the center, leading to greater undercooling and enhanced nucleation; meanwhile, the dendritic arms are broken, which results in the finer grain size and the uniform distribution of the Zn-rich $Mg_{17}Al_{12}$ phases (Figures 6(c) through (f) and 8(c) through (f)). Simultaneously, compulsive convection makes possible the formation of a uniform solute concentration filed across the billet section, which reduces the deflection of the solute elements during the growth of dendrites and eliminates the macrosegregation (Figures 6(c) through (f)). As can be seen from Figures 8(c) through (f), it is found that the addition of the Ti grain refiner can reduce the grain size further. For the AZ31-0.01Ti alloy (30 Hz and 80 A), the grain size in the billet center is smaller than that at the edge, which is the same as is found in the conventional casting condition (Figure 3 for the AZ31-0.01Ti alloy); this can be explained by a cooling rate at the edge that is higher than 6 K/s.

### C. Mechanical Properties

The Ti effect on the mechanical properties is consistent with the different grain sizes of the alloys, *i.e.*, the finer grain size corresponds to a higher yield strength and elongation (Figures 6(a) and (b)). As shown in Figure 13, yield strength ($\sigma_y$) is a function of grain size, which is consistent with the Hall–Petch formula and can be expressed as $\sigma_y = 39.31 + 142.53d^{-1/2}$ for the conventional casting ingots solidified at a cooling rate of 6 K/s. For the DC and LFEC billets, the relationship between yield strength and grain size (in the center of billets) can be described as $\sigma_y = 51.53 + 90.85\ d^{-1/2}$. Compared with the Sr-refining AZ31 alloy,[6] it can be seen that adding grain refiner (Sr and Ti) has a small effect on the intercept of the ordinate of yield strength, but a large effect of the physical grain refinement (DC and LFEC).

### V. CONCLUSIONS

1. Small Ti additions can effectively refine the grain of AZ31 magnesium alloy, and the effect is sensitive to
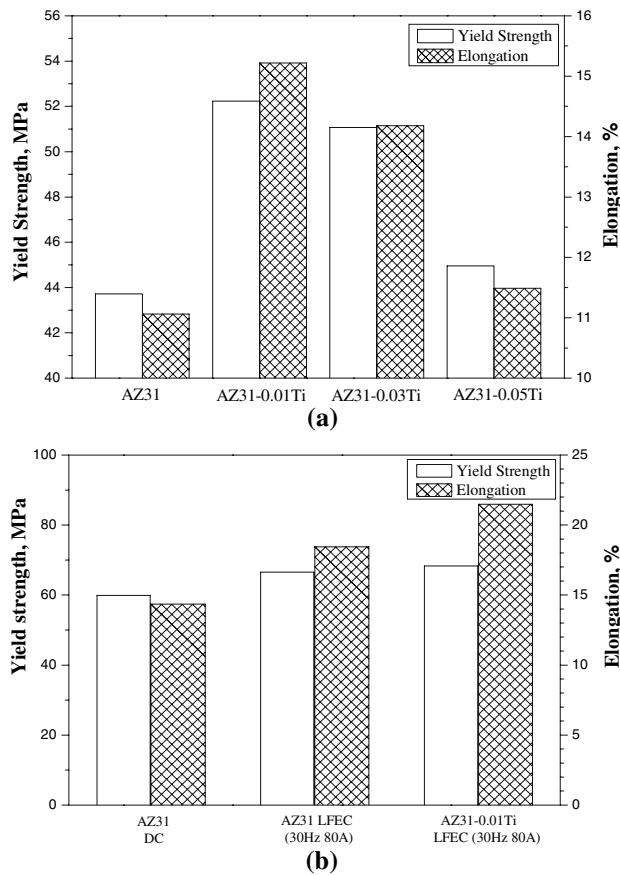
(a)


(b)

Fig. 9—Mechanical properties of (a) the as-cast alloys solidified at a cooling rate of 6 K/s and (b) the DC and LFEC AZ31 alloys tested at room temperature.
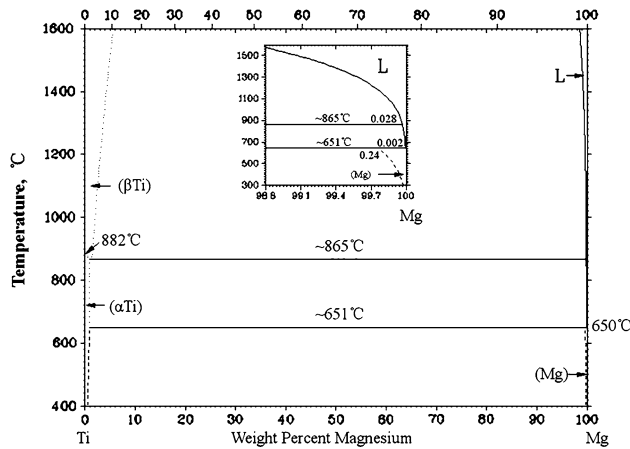

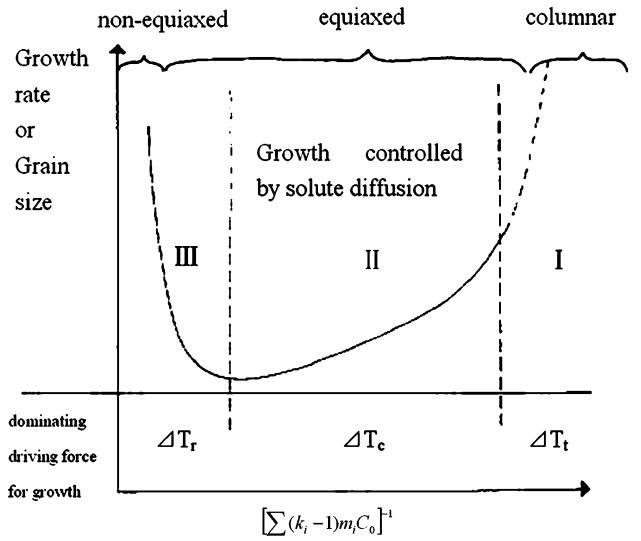Fig. 10—Binary phase diagram of Mg-Ti system.


Fig. 11—A sketch showing how the average dendritic growth rate (and grain size) varies over the composition range. The solute concentration increases to the left in the figure.[17]
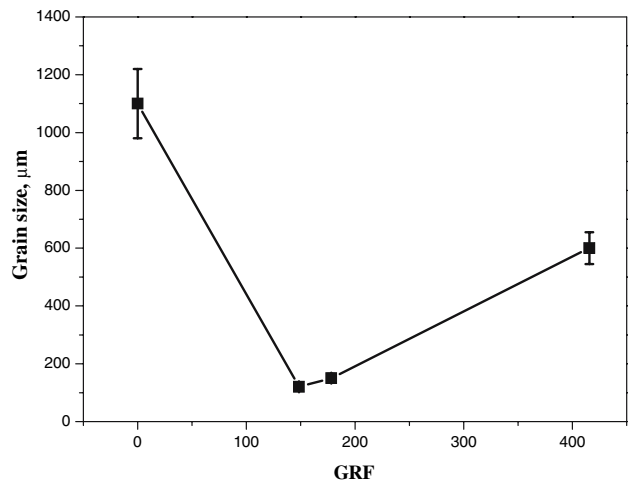

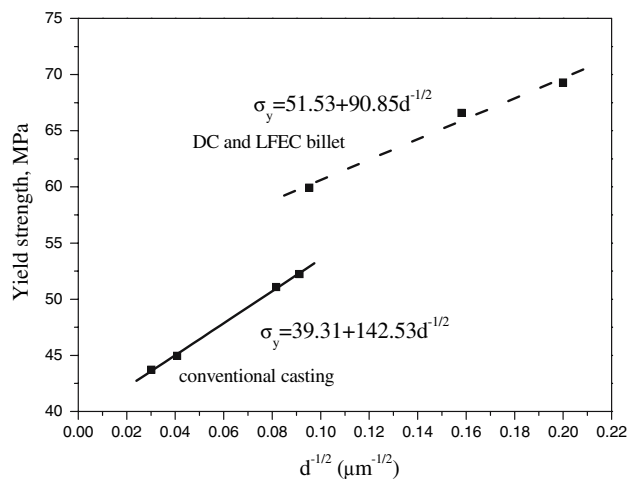Fig. 12—Graph of grain size plotted against the GRF for the investigated AZ31 alloys.


Fig. 13—Yield strength as a function of grain size ($d^{-1/2}$).

the cooling rate. For a given composition, the grain size decreases with an increasing cooling rate, and grain size decreases first, then increases slightly for Ti-containing AZ31 alloys; for a given cooling rate, the grain size decreases first, and then increases with an increasing Ti content.

2. Ti additions have no effect on the formation and distribution of secondary phases for the conventional-cast AZ31 alloy. For the DC-cast AZ31 billet, the microstructure in the center is composed of relatively coarse dendrites and larger Zn-rich $\beta$-phases in the interdendritic regions; at the edge, a more equiaxed grain structure is evident and the Zn-rich $\beta$-phases are more refined. For the LFEC billet, all Zn-rich $\beta$-phases are greatly refined across the billet cross section, with a size of approximately 3 to 4 $\mu$m, and show a uniform distribution in the $\alpha$(Mg) matrix.

3. The yield strength of AZ31 alloy can be improved as a result of grain refinement through Ti additions and can be expressed by the Hall–Petch formula with $\sigma_y = 39.31 + 142.53 d^{-1/2}$; the combination of a Ti grain refiner and the LFEC process can further improve the yield strength, and the relationship between yield strength and grain size can be described as $\sigma_y = 51.53 + 90.85\ d^{-1/2}$. On the other hand, the finest grain size corresponds to the highest elongation.

## REFERENCES

1. T.C. Chang, J.Y. Wang, and O. Lee: *J. Mater. Process. Technol.*, 2003, vol. 140, pp. 588–91.
2. A.A Luo: SAE Technical Paper 2005-01-0734, Society for Automotive Engineers International, Warrendale, PA, 2005, pp. 411–21.
3. V. Kaese, L. Greve, S. Jutter, M. Goede, S. Schumann, H. Friedrich, W. Holl, and W. Ritter: *Proc. 6th Int. Conf. Magnesium Alloys and Their Applications*, K.U. Kainer, ed., Wiley-VCH, Weinheim, Germany, 2003, pp. 949–54.
4. Y.X. Wang, X.Q. Zeng, and W.J. Ding: *Scripta Mater.*, 2006, vol. 54, pp. 269–73.
5. D.H. St John, M. Qian, M.A. Easton, P. Cao, and Z. Hildebrand: *Metall. Mater. Trans. A*, 2005, vol. 36A, pp. 1669–79.
6. Y.X. Wang, X.Q. Zeng, W.J. Ding, A.A. Luo, and A.K. Sachdev: *Metall. Mater. Trans. A*, 2006, vol. 37A, pp. 1333–41.
7. J. Dong, J.Z. Cui, F.X. Yu, C.Y. Ban, and Z.H. Zhao: *Metall. Mater. Trans. A*, 2004, vol. 35A, pp. 2487–94.
8. S.J. Guo, Q.C. Le, Z.H. Zhao, Z.J. Wang, and J.Z. Cui: *Mater. Sci. Eng.*, 2005, vol. 404A, pp. 323–29.
9. J.Z. Cui, Q.C. Le, S.J. Guo, X.J. Zhang, and Z.H. Zhao: *China Materials Forum 2002*, CMS, Beijing, China, 2002, pp. 26–33.
10. M. Easton and D.H. St John: *Metall. Mater. Mater. Trans. A*, 1999, vol. 30A, pp. 1625–33.
11. F. Xue, W.W. Du, and Y.S. Sun: *Mater. Sci. Forum*, 2005, vols. 488–489, pp. 143–46.
12. Y.X. Wang: Doctoral Paper, Shanghai Jiao Tong University, Shanghai, P.R. China, 2006.
13. M. Johnsson and L. Bäckerud: *Z. Metallkd.*, 1996, vol. 87, pp. 216–20.
14. Y.C. Lee, A.K. Dahle, and D.H. St John: *Metall. Mater. Trans. A*, 2000, vol. 31A, pp. 2895–906.
15. J.L. Murray: *Bull. Alloy Phase Diagrams*, 1986, vol. 7, pp. 245–48.
16. J. Lipton, M.E. Glicksman, and W. Kurz: *Mater. Sci. Eng.*, 1984, vol. 65A, pp. 57–63.
17. M. Johnsson: *Thermochimica Acta*, 1995, vol. 256, pp. 101–21.
18. M. Easton and D.H. St John: *Metall. Mater. Trans. A*, 1999, vol. 30A, pp. 1613–24.